Optimize the thermoelectric performance of CdO ceramics by doping Zn*

Xin-Yu Zha(查欣雨), Lin-Jie Gao(高琳洁)†, Hong-Chang Bai(白洪昌), Jiang-Long Wang(王江龙)‡, and Shu-Fang Wang(王淑芳)

Hebei Key Laboratory of Optic-electronic Information and Materials, The College of Physics Science and Technology, Hebei University, Baoding 071002, *China*

(Received 19 April 2017; revised manuscript received 26 July 2017; published online 10 September 2017)

The thermoelectric performance of CdO ceramics was enhanced by simultaneously optimizing the electrical and thermal transport properties via a small amount of Zn doping (≤3%). The introduction of Zn can obviously increase the electrical conductivity of CdO due to the simultaneous increase of carrier concentration and mobility, and eventually results in an improvement in power factor. Zn doping is also effective in suppressing the thermal conductivity of CdO because of stronger phonon scatterings from point defects, Zn-riched second phase, and grain boundaries. A best *ZT* of about 0.45 has been achieved in the $Cd_{1-x}Zn_xO$ systems at about 1000 K, which is comparable to the highest values reported for other n-type oxide TE materials.

Keywords: thermoelectric properties, CdO, Zn doping, power factor, thermal conductivity

PACS: 72.80.Ga, 72.20.Pa, 81.20.Ev **DOI:** 10.1088/1674-1056/26/10/107202

1. Introduction

Rapid depletion of fossil fuels and growing environmental concerns promote the fast development of clean energy materials all over the world. Thermoelectric (TE) materials can realize the direct conversion between thermal energy and electric energy, and therefore have attracted increasing attentions.[1–7] The performance of a thermoelectric material can be evaluated by the dimensionless figure of merit $ZT = (S^2\sigma/\kappa)T$, where S is the Seebeck coefficient, σ is the electrical conductivity, T is the absolute temperature, and κ is the thermal conductivity which mainly includes the carrier thermal conductivity κ_e and the phonon thermal conductivity κ_{ph}. The key to realize large scale application of thermoelectric technique is to obtain high *ZT* material, by optimizing the power factor $S^2\sigma$ or suppressing the thermal conductivity κ of the material.

Oxides have many advantages for thermoelectric applications due to their good thermal/chemical stability in air, low cost, and simple fabrication process. Last decade has witnessed a great progress on p-type oxide TE materials, but the *ZT* values of n-type oxides are still low.[8–14] It is well known that the TE models require the integration of p-type and n-type TE materials Therefore, the issue of how to improve the TE performance of n-type oxides became a challenge for researchers. Extensive studies have been carried out on the n-type oxide TE materials such as $SrTiO_3$, $CaMnO_3$, ZnO, In_2O_3, etc., and so far a highest *ZT* of about 0.47 has been achieved in the Al/Ga co-doped ZnO samples at about 1000 K.[15–22] CdO belongs to the same family of transparent conductive oxides as ZnO or In_2O_3. Recent studies showed that the pristine CdO ceramic samples even possessed higher *ZT* values than the corresponding ZnO and In_2O_3 ceramics and appropriate element doping can further increase the TE performance, suggesting the great potential application of CdO for TE devices.[23–26] In this paper, we report the improvement of TE performance of CdO ceramics by simultaneously optimizing the electrical and thermal transport properties via a small amount of Zn doping (≤3%). A high *ZT* of about 0.45 has been achieved in the optimal Zn-doped CdO sample at about 1000 K, which is 32% higher than that of the pristine CdO and is also comparable to the highest values reported for the state-of-art n-type oxide TE materials.

2. Experimental section

$Cd_{1-x}Zn_xO$ ($x = 0$, 0.5%, 1%, 2%, 3%) ceramic samples were synthesized with the solid state reaction method by using the commercial CdO powders (Alfa Aesar, 98.9%) and ZnO powders (Tianjin Kemiou, 99.9%) as the starting materials. The mixed powders of CdO and ZnO were wet grinded in air for 4 hours by a ball-milling machine, dried at 358 K for 4 hours and pressed into pellets with a diameter of 14 mm under 230 Mpa at room temperature. Then the pellets were

*Project supported by the National Natural Science Foundation of China (Grant No. 51372064), the Natural Science Foundation of Hebei Province, China (Grant Nos. A2014201176 and E2017201209), the Outstanding Doctoral Cultivation Project of Hebei University (Grant No. YB201502), and the Hebei Province Universities Science and Technology Program funded by the Hebei Provincial Education Department, China (Grant Nos. ZD2014018 and QN2017017).

†Corresponding author. E-mail: LinjieGao@hotmail.com

‡Corresponding author. E-mail: jlwang@hbu.edu.cn

© 2017 Chinese Physical Society and IOP Publishing Ltd

sintered in a Muffle furnace in the air. The typical sintering process included a fast heating to 1173 K with the rate of about 10 K/min, followed by holding at 1173 K for 20 hours, and then a slow cooling with the rate of 1 K/min to 473 K before naturally cooled to room temperature. Finally, polycrystalline specimens with nominal compositions of $Cd_{1-x}Zn_xO$ ($x = 0$, 0.5%, 1%, 2%, 3%) were obtained.

The crystalline phase and the grain size of the $Cd_{1-x}Zn_xO$ samples were analyzed by powder x-ray diffraction (XRD) with Cu Kα radiation (Bruker D8 Advance). The microstructure and composition of the samples were inspected by the field-effect scanning electron microscope (FESEM, FEI Nova Nano SEM 450) coupled with an energy-dispersive x-ray (EDX) detector. The room temperature carrier concentration n and mobility μ were measured using the Van der Pauw method with a Hall effect measurement system (ECT, ET-9000). The electrical conductivity σ and Seebeck coefficient S were simultaneously measured on a Linseis LSR-800 measurement system by the standard dc four-probe technology in the temperature range of 300 K–1000 K. The thermal conductivity κ was calculated from $\kappa = DC_pd$, where the thermal diffusivity coefficient (D) was obtained by the laser flash diffusivity method on a Linseis LFA1000 system, the specific heat capacity C_p was measured using the differential scanning calorimeter (Netzsch DSC200F3), and the bulk density d was measured by the dimensions and mass of the samples and then reconfirmed by the Archimedes method.

3. Results and discussion

Figure 1(a) shows the XRD patterns of $Cd_{1-x}Zn_xO$ ceramic samples. The CdO phase with a space group Fm-3m (225) can be well indexed by matching the diffraction peaks with the available database (PDF #750594). As the Zn doping content increases, the peak position of $Cd_{1-x}Zn_xO$ shifts to higher angle (as seen in the inset of Fig. 1(a)), suggesting the lattice parameters decrease with the increase of Zn doping. We calculate the lattice parameters of these samples, which are presented in Fig. 1(b). The reduction of lattice parameters can be resulted from the substitution of Zn^{2+} for Cd^{2+}, as the ionic radius of Zn^{2+} (0.74 Å) is smaller than that of Cd^{2+} (0.97 Å). We also estimated the average grain size of each sample by using the Scherer formula, and found the average grain size of $Cd_{1-x}Zn_xO$ decreases with the increase of Zn doping. It is known that to preserve fine grains during the sintering process of ceramics, a second phase can be added into the material to pin grain boundaries.[27,28] So the reduction of average grain size in the Zn-doped samples could be attributed to the grain boundary pinning effect of the Zn dopant. It is worth mentioning here that although no diffraction peaks related to the impurities are observed in Fig. 1(a) due to the detection limit of XRD, we cannot exclude the presence of very small amount of second phase in the samples, especially in the samples with higher Zn doping content. To confirm the speculation, we performed the EDS element mapping measurements on the 3% Zn-doped sample, which is provided in Fig. 2. It can be clearly seen that there indeed exists the Zn-riched second phase in this sample.

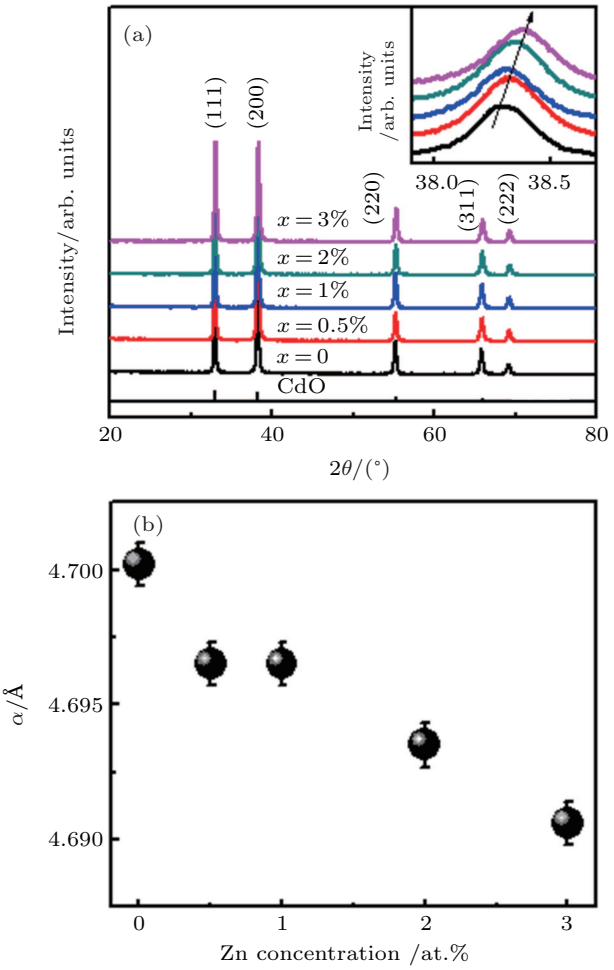


Fig. 1. (color online) (a) XRD patterns and (b) lattice parameters of $Cd_{1-x}Zn_xO$ ($x = 0$, 0.5%, 1%, 2%, 3%) samples. The inset of Fig. 1(a) is the magnified curves of (200) diffraction peak of the $Cd_{1-x}Zn_xO$ samples. Standard diffraction peaks of CdO are also provided in Fig. 1(a) for comparison.

The Hall measurements show that all $Cd_{1-x}Zn_xO$ samples are n-type. Figure 3 displays the dependence of carrier concentration n and mobility μ of $Cd_{1-x}Zn_xO$ samples on the Zn doping content. Both n and μ increase with the Zn doping content. It was reported that when doping Zn^{2+} into CdO, Zn^{2+} may have the following effects: the substitution of Cd^{2+}, the occupation of the interstitial positions or Cd^{2+} vacancies, and the aggregation on CdO grains in form of Zn-riched second phase.[29] The increment of n with Zn doping content in this work implies that most of Zn ions occupy the interstitial positions or Cd^{2+} vacancies in the CdO lattice, which can behave as donors and contribute electron carriers. Figure 3 shows the mobility μ also increases with the doping content. The simultaneous increase in carrier concentration and mobility with increasing the doping concentration was also found in Al-doped

ZnO and Sn or Dy-doped CdO.[30–32] In these samples, the grain boundary scattering is the dominant scattering mechanism. According to this mechanism, the increase of carrier concentration can lower the potential barrier height of grain boundaries, which makes it easier for charge carriers to move across grain boundaries and finally leads to an increase of mobility.

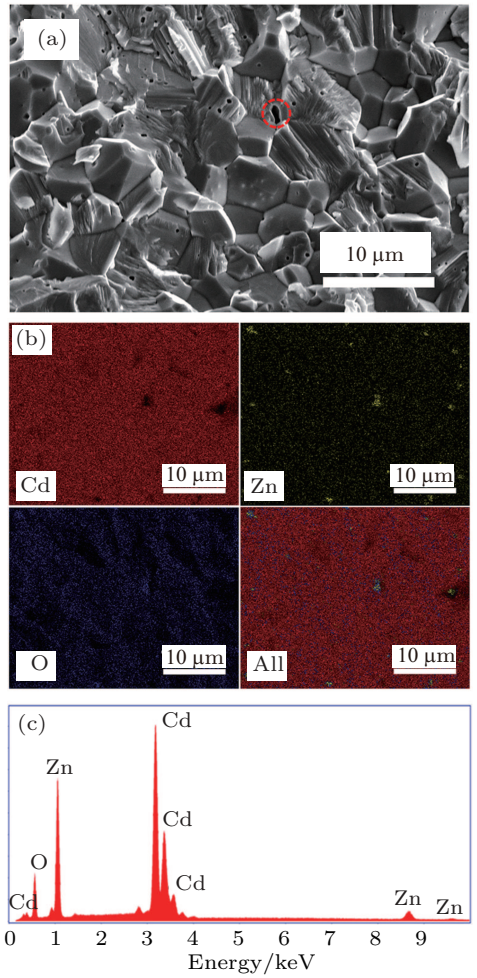


Fig. 2. (color online) (a) The fractured cross-sectional SEM micrographs and (b) the corresponding element mappings of the $Cd_{0.97}Zn_{0.03}O$ sample. (c) EDS spectrum of the Zn-riched particles marked in Fig. 2(a).

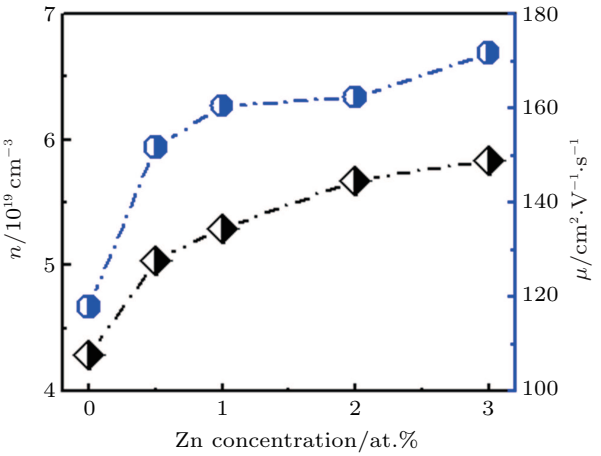


Fig. 3. (color online) Carrier concentration n and mobility μ of $Cd_{1-x}Zn_xO$ ($x = 0$, 0.5%, 1%, 2%, 3%) samples measured at room temperature.

Figure 4(a) shows the temperature dependence of the electrical conductivity σ of these $Cd_{1-x}Zn_xO$ samples. From the figure we can clearly see that the electrical conductivity σ of all samples decreases with the increase of temperature, exhibiting a heavily-doped semiconducting behavior. Moreover, the electrical conductivity σ of all doped samples is higher than that of the pristine CdO and the value of σ increases gradually with the doping content due to the increased carrier concentration and mobility. Figure 4(b) presents the Seebeck coefficient S of these $Cd_{1-x}Zn_xO$ samples as a function of temperature. Each sample shows a negative S in the whole

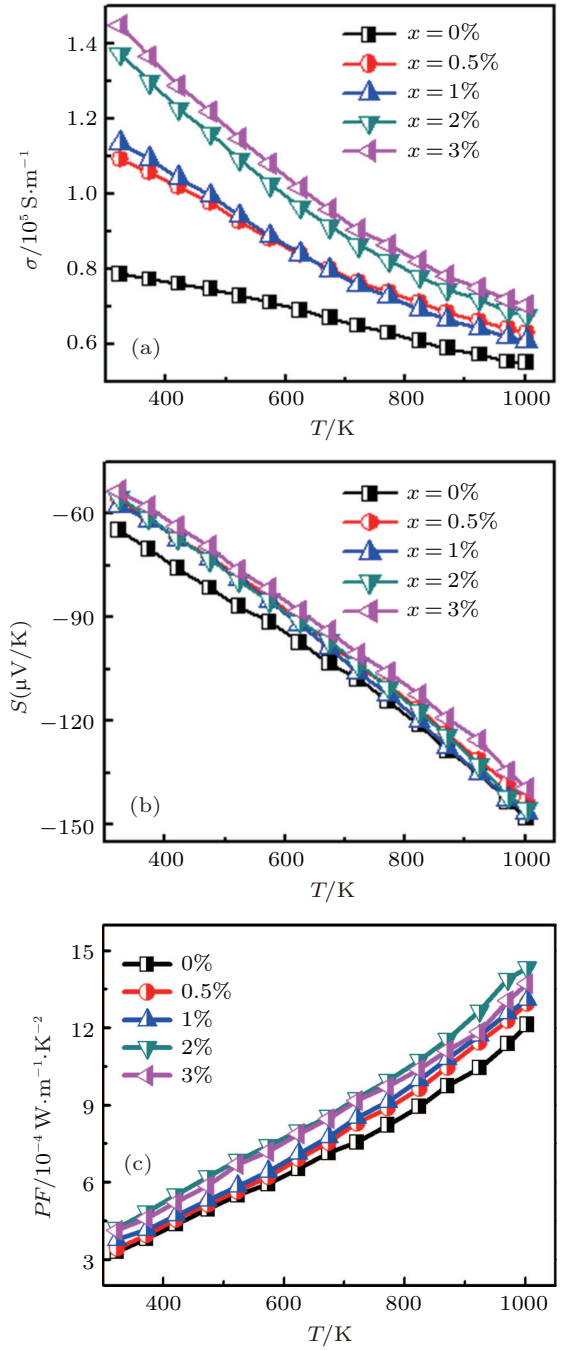


Fig. 4. (color online) Temperature dependence of (a) electrical conductivity σ, (b) Seebeck coefficient S, and (c) power factor of $Cd_{1-x}Zn_xO$ ($x = 0$, 0.5%, 1%, 2%, 3%) samples.

measured temperature range, indicating that these samples are all n-type conducting, which is consistent with the Hall measurement. The absolute Seebeck coefficient $|S|$ of these samples are found to increase with the temperature, which is also a typical behavior of the heavily doped n-type semiconductors. For the heavily doped n-type semiconductors, the Seebeck coefficient can be described by[33,34]

$$|S| = \frac{4\pi^2 k_B^2}{eh^2}\left(\frac{\pi}{3n}\right)^{2/3} m^* T, \quad (1)$$

where k_B is the Boltzmann constant, h is the Planck constant and m^* is the carrier effective mass. Based on the above equation, $|S|$ is inversely proportional to the carrier concentration n, and therefore the value of $|S|$ of $Cd_{1-x}Zn_xO$ samples decreases with the Zn doping content. We calculated the power factor PF of these $Cd_{1-x}Zn_xO$ samples according to the above data of σ and S, which is shown in Fig. 4(c), and the result revealed that doping Zn can obviously improve the power factor of CdO sample. For example, the 3% Zn-doped sample has the PF of about 1.37×10^{-3} W·m^{-1}·K^{-2} at 1000 K, ~13.2% higher than that of the pristine CdO.

Figure 5(a) shows the temperature dependence of the total thermal conductivity κ of the $Cd_{1-x}Zn_xO$ samples. The κ values of all samples decrease as the temperature increases. In addition, doping Zn into CdO can greatly suppress the value of κ, which decreases from 8.1 W·m^{-1}·K^{-1} to 5.9 W·m^{-1}·K^{-1} at room temperature and from 3.6 W·m^{-1}·K^{-1}~2.9 W·m^{-1}·K^{-1} at 1000 K. To estimate the contribution of carriers and phonons to the total thermal conductivity κ of $Cd_{1-x}Zn_xO$ system, we plot the temperature dependence of electric thermal conductivity κ_e and phonon thermal conductivity κ_{ph}, respectively, as shown in Figs. 5(b) and 5(c). Here κ_e is calculated using the Wiedeman–Franz law, and κ_{ph} is derived directly by subtracting κ_e from κ. It is obvious that the contribution of electric thermal conductivity to the total thermal conductivity is small, and κ is mainly determined by the phonon thermal conductivity. As can be seen from Fig. 5(c), the phonon thermal conductivity of the $Cd_{1-x}Zn_xO$ samples decreases with the increasing Zn content, at 1000 K, the value of κ_{ph} of the 3% doped sample is only about 1.2 W·m^{-1}·K^{-1}, a remarkable reduction as compared to the pristine CdO and is very close to the amorphous limit of CdO that calculated by the Cahill's formulation. Several factors might be responsible for the significant suppression in κ_{ph} of the Zn-doped CdO ceramics. Firstly, the replacements of Cd^{2+} by Zn^{2+} and the insertion of Zn^{2+} in the interstitials positions or Cd^{2+} vacancies can introduce a large amount of point defects to the CdO lattice. These point defects can effectively scatter the short-wavelength phonons and lead to a decrease of κ_{ph}; Secondly, the Zn-riched second phase with the dimension of sub-micrometers, as can be identified from the SEM measurements shown in Fig. 2, can serve as the scattering centers of the long or middle-wavelength phonons; Thirdly, the reduced grain size of the doped samples results in an increment in grain boundaries, and thus enhanced scatterings for the long-wavelength phonons.

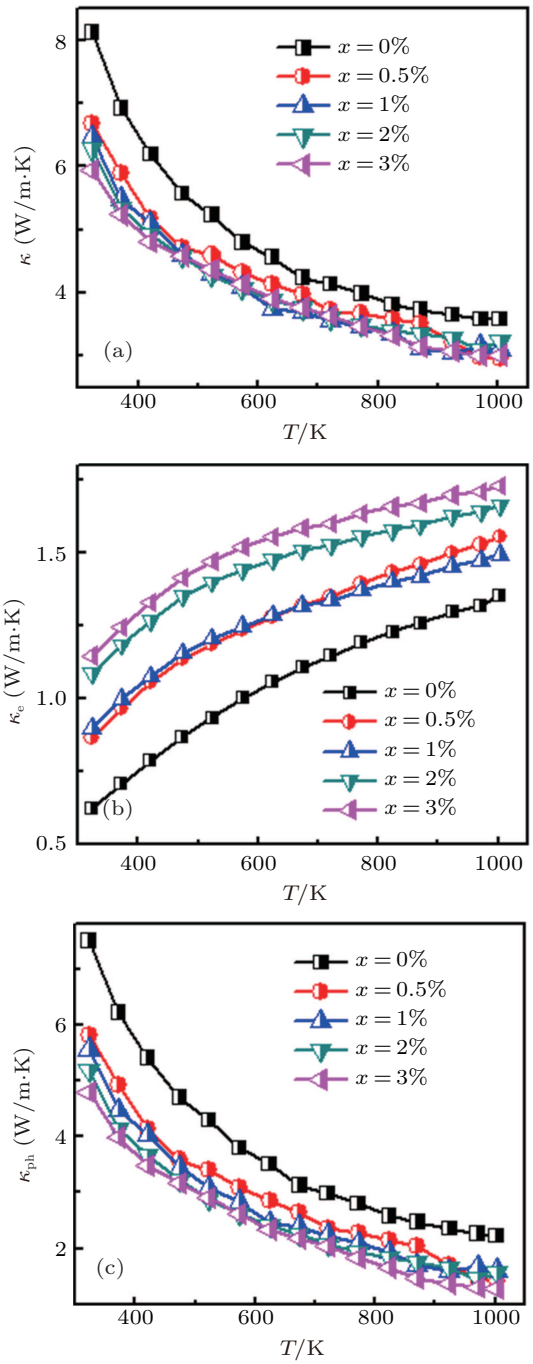


Fig. 5. (color online) Temperature dependence of (a) total thermal conductivity κ, (b) electronic thermal conductivity κ_e, (c) phonon thermal conductivity κ_{ph} of $Cd_{1-x}Zn_xO$ ($x = 0, 0.5\%, 1\%, 2\%, 3\%$) samples.

The temperature dependence of ZT for the $Cd_{1-x}Zn_xO$ samples is shown in Fig. 6. In the whole measured temperature range, the ZT value of each sample increases monotonically with the temperature. Benefiting from the improved power factor and the decreased thermal conductivity, all doped samples show higher ZT values than the pristine CdO. A highest ZT of 0.45 is achieved at 1000 K for the optimal doped

sample of $Cd_{0.97}Zn_{0.03}O$, which is comparable to the best *ZT* value obtained in the state-of-art n-type oxide TE materials, the best result reported in n-type In_2O_3 bulk ceramics is 0.44 at 923 K,[22] and the ZT of 0.47 at 1000 K is also the highest value reported in n-type ZnO bulks.[17] It is worthy to mention here that higher doping content cannot continue to optimize the *ZT* due to the obvious decrease of power factor resulted form more second phases.

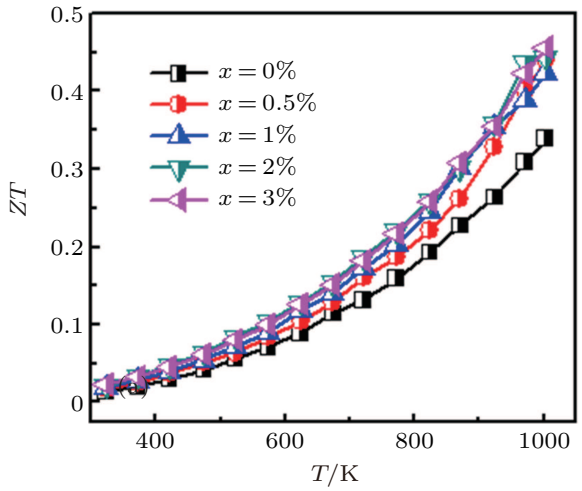


Fig. 6. (color online) Temperature dependence of *ZT* of $Cd_{1-x}Zn_xO$ ($x = 0$, 0.5%, 1%, 2%, 3%) samples.

4. Conclusion

$Cd_{1-x}Zn_xO$ ($x = 0$, 0.5%, 1%, 2%, 3%) ceramic samples were synthesized by the conventional solid state reaction method. The introduction of Zn had significant influence on the electrical and thermal transport properties of CdO. The carrier concentration and mobility of the samples were found to increase simultaneously with Zn content, led to increment in electrical conductivity and thus enhanced power factor for all Zn-doped samples. Doping of Zn can also suppress the thermal conductivity of CdO through enhanced phonon scatterings from point defects, Zn-riched second phase and grain boundaries. Benefiting from the synergetic optimization in electrical and thermal transport properties, the *ZT* value was greatly improved from 0.34 for the pristine CdO to 0.45 for the 3% doped sample. The results demonstrate that doping Zn is an effective strategy to enhance the TE performance of CdO ceramics and the great potential of these Zn-doped CdO samples as the promising n-type oxide TE materials.

References

[1] Bell L E 2008 *Science* **321** 1457
[2] Zhao J, Liu Z, Reid J, Takarabe K, Iida T, Wang B, Yoshiya U and Tse J S 2015 *J. Mater. Chem.* **3** 19774
[3] Zhao L D, Lo S H, Zhang Y, Sun H, Tan G, Uher C, Wolverton C, Dravid V P and Kanatzidis M G 2014 *Nature* **508** 373
[4] Zhang X X, Chang C, Zhou Y M and Zhao L D 2017 *Materials* **10** 198
[5] Liu Y, Zhao L D, Zhu Y C, Liu Y C, Li F, Yu M J, Liu D B, Xu W, Lin Y H and Nan C W 2016 *Adv. Energy Mater.* **6** 1502423
[6] Feng D, Zheng F S, Wu D, Wu M H, Li W, Huang L, Zhao L D and He J Q 2016 *Nano Energy* **27** 167
[7] Bittner M, Helmich L, Nietschke F, Geppert B, Oeckler O and Feldhoff A 2017 *J. Eur. Ceram. Soc.* **37** 3909
[8] Lan J L, Liu Y C, Zhan B, Lin Y H, Zhang B, Yuan X, Zhang W Q and Nan C W 2013 *Adv. Mater.* **25** 5086
[9] Nong N V, Pryds N, Linderoth S and Ohtaki M 2011 *Adv. Mater.* **23** 2484
[10] Wang S F, Zhang Z C, He L P, Chen M J, Yu W and Fu G S 2009 *Appl. Phys. Lett.* **94** 162108
[11] Zhao L D, He J Q, Berardan D, Lin Y H, Li J F, Nan C W and Dragoe N 2014 *Energy Environ. Sci.* **7** 2900
[12] Kumar P, Kashyap S C, Sharma V K and Gupta H C 2015 *Chin. Phys. B* **24** 098101
[13] Wu Z H, Xie H Q, Zhai Y B, Gan L H and Liu J 2015 *Chin. Phys. B* **24** 034402
[14] Li L L, Qin X Y, Liu Y F and Liu Q Z 2015 *Chin. Phys. B* **24** 067202
[15] Wang H C, Wang C L, Su W B, Liu J, Sun Y, Peng H and Mei L M 2011 *J. Am. Caram. Soc.* **94** 838
[16] Bocher L, Aguirre M H, Logvinovich D, Shkabko A, Robert R, Trottmann M and Weidenkaff A 2008 *Inorg. Chem.* **47** 8077
[17] Ohtaki M, Araki K and Yamamoto K 2009 *J. Electron. Mater.* **38** 1234
[18] Jood P, Mehta R J, Zhang Y L, Tasciuc T B, Dou S X, Singh D J and Ramanath G 2014 *RSC Adv.* **4** 6363
[19] Teranishi T, Mori Y, Hayashi H and Kishimoto A 2012 *J. Am. Ceram. Soc.* **95** 690
[20] Liu Y, Lin Y H, Lan J L, Xu W, Zhang B P, Nan C W and Zhu H M 2010 *J. Am. Ceram. Soc.* **93** 2938
[21] Berardan D, Guilmeau E, Maignan A and Raveau B 2008 *Solid State Commum.* **146** 97
[22] Lan J L, Liu Y, Lin Y H, Nan C W, Cai Q and Yang X 2015 *Sci. Rep.* **5** 7783
[23] Wang S F, Liu F Q, Lü Q, Dai S Y, Wang J L, Yu W and Fu G S 2013 *J. Eur. Ceram. Soc.* **33** 1763
[24] Wang S F, Lü Q, Li L J, Fu G S, Liu F Q, Dai S Y, Yu W and Wang J L 2013 *Scr. Mater.* **69** 533
[25] Li L J, Liang S, Li S M, Wang J L, Wang S F, Dong G Y and Fu G S 2014 *Nanotechnology* **25** 425402
[26] Gao L J, Wang S F, Liu R, Zhai S J, Zhang H R, Wang J L and Fu G S 2016 *J. Alloys Compd.* **662** 213
[27] Cinibulk M K 2004 *J. Am. Ceram. Soc.* **87** 692
[28] Granger G B and Guizard C 2007 *Scr. Mater.* **56** 983
[29] Dakhel A A 2012 *J. Alloys Compd.* **539** 26
[30] Wiff J P, Kinemuchi Y, Kaga H, Ito C and Watari K 2009 *J. Eur. Ceram. Soc.* **29** 1413
[31] Yan M, Lane M, Kannewurf C R and Chang R P H 2001 *Appl. Phys. Lett.* **78** 2342
[32] Dakhel A A 2009 *Sol. Energy* **83** 934
[33] Jung K H, Lee K H, Seo W S and Choi S M 2012 *Appl. Phys. Lett.* **100** 253902
[34] Tsujii N and Mori T 2013 *Appl. Phys. Exp.* **6** 043001